

Short Communication

Effects of $Ti_3C_2T_x$ nano-sheets (MXenes) on the microstructural and electrochemical properties of SnO_2/Ti anodes

Sergio González-Poggini¹, Andreas Rosenkranz¹, Bo Wang², Samuel Hevia³, Jinhong Yu²,
Melanie Colet-Lagrille^{1,*}

¹ Department of Chemical Engineering, Biotechnology and Materials, Faculty of Physical and Mathematical Sciences, Universidad de Chile, Beauchef 851, Santiago, Chile

² Key Laboratory of Marine New Materials and Related Technology, Zhejiang Key Laboratory of Marine Materials and Protection Technology, Ningbo Institute of Material Technology & Engineering, Chinese Academy of Sciences, Ningbo 315201, People's Republic of China

³ Instituto de Física y Centro de Investigación en Nanotecnología y Materiales Avanzados, Pontificia Universidad Católica de Chile, Macul, Santiago, Chile

*E-mail: mcolet@ing.uchile.cl

Received: 15 December 2020 / Accepted: 5 February 2021 / Published: 31 March 2021

The effects of the incorporation of $Ti_3C_2T_x$ nano-sheets (MXenes) on the microstructure of SnO_2/Ti electrodes and their electro-oxidation catalytic activity for the degradation of methyl red is studied in this work. MXenes- SnO_2/Ti electrodes are fabricated by spin-coating followed by a thermal treatment under ambient atmospheric conditions using a solution containing MXene nano-sheets, $SnCl_2$, citric acid and ethylene glycol as precursor. Energy-dispersive X-ray spectroscopy, Raman spectroscopy and X-ray diffraction analyses of the MXenes- SnO_2/Ti electrodes surface indicate the formation of SnO_2-TiO_2 films with Ti^{4+} ions incorporated into the lattice of SnO_2 crystals. Cyclic voltammetry curves demonstrate that the oxygen evolution reaction is restrained by the MXenes- SnO_2/Ti electrodes, while the methyl red electro-oxidation is enhanced – with kinetics following a pseudo-first-order model – compared to the performance of (pure) SnO_2/Ti electrodes. These results suggest that oxygen vacancies are formed in the crystal lattice of MXenes- SnO_2/Ti electrodes, which act as charge carriers and increase the electrical conductivity of SnO_2 as confirmed by the lower charge transfer resistance of MXenes- SnO_2/Ti electrodes determined by electrochemical impedance spectroscopy analysis.

Keywords: 2d materials; $Ti_3C_2T_x$ nano-sheets; anodic oxidation; SnO_2 -based electrodes; water treatment

1. INTRODUCTION

In recent years, electrochemical advanced oxidation processes (EAOPs) have received considerable attention for wastewater treatment. EAOPs are based upon the electrochemical in-situ

production of highly reactive hydroxyl radicals ($\bullet\text{OH}$), which non-selectively react with a large variety of organic molecules thus degrading even extremely recalcitrant compounds [1,2]. In this context, various metal oxide-coated anodes have been studied for anodic oxidation of pollutants in wastewater exhibiting excellent electrocatalytic activity. Among these, SnO_2 -based anodes have shown a high electrocatalytic activity for the generation of hydroxyl radicals that, together with their affordability and easiness for fabrication, makes them a promising alternative to conventional EAOPs anode materials such as boron-doped diamond, IrO_2 and RuO_2 . Different approaches have been employed to increase the catalytic activity of SnO_2 -coated anodes, including their doping with metals/non-metals atoms, different fabrication techniques and the incorporation of interface layers of other metal oxides [3]. Additionally, previous studies have revealed the importance of the crystalline structure of SnO_2 -based anodes on their electro-oxidation performance. For instance, the insertion of Sb and Nb dopants in the structure of SnO_2 considerably enhanced the lifetime of Ti/SnO_2 anodes. Furthermore, the conductivity has been significantly improved with the incorporation of dopants such as Sb and fluoride ions [4,5].

$\text{Ti}_3\text{C}_2\text{T}_x$ nano-sheets (MXenes) correspond to a new class of layered 2d materials, which have been identified as promising co-catalysts for applications such as environmental remediation, batteries and supercapacitors, due to their high surface area and excellent electronic conductivity [6,7]. MXenes are composed of early transition metal carbides/nitrides (Ti carbides in the case of this work), usually produced by selectively removing the A layers from $\text{M}_{n+1}\text{AX}_n$ phases, for which M stands for an early transition metal, A is mainly a group IIIA or IVA (i.e., group 13 or 14) element, X represents C and/or N, and n is equal to 1, 2 or 3. The thermal treatment of MXenes in oxygen atmospheres generally leads to the formation of anatase and rutile TiO_2 nano-crystals [8,9], which may be interesting for catalytic applications [10,11]. Recent studies have shown the potential of MXenes-based electrodes for water splitting and hydrogen production; particularly, the combinations of Ti_3C_2 -MXenes with MoSe_2 or Ni-Fe have demonstrated high catalytic activity and durability during electrochemical water splitting [12–14]. To the best of our knowledge, neither the effects of the incorporation of MXenes on the SnO_2 microstructure nor the performance of MXenes- SnO_2/Ti electrodes in electrocatalytic applications have been reported yet.

Consequently, this work addresses: (i) the surface characterization of stable MXenes- SnO_2 electrodes fabricated by spin coating of a precursor solution on Ti substrates, and (ii) the effects of the incorporation of MXenes to the SnO_2/Ti electrodes nanostructure on their electrocatalytic activity for the oxygen evolution reaction and the electro-oxidation of methyl red.

2. EXPERIMENTAL

2.1. Synthesis of $\text{Ti}_3\text{C}_2\text{T}_x$ nano-sheets (MXenes)

Ti_3AlC_2 -powder purchased from FORSMAN SCIENTIFIC Co. Ltd. (Beijing, China) was used to synthesize multi-layer $\text{Ti}_3\text{C}_2\text{T}_x$ nano-sheets. Therefore, 10 g of the Ti_3AlC_2 -powder were immersed under stirring in 100 mL of a 40% hydrofluoric acid solution (24 hours at room temperature). The prepared suspension was subsequently washed using deionized water until reaching a pH above 6 and,

afterwards, centrifuged to separate the powder sections. Finally, the washed powder was filtered under vacuum conditions and dried at room temperature for 24 hours in a vacuum oven.

2.2. Characterization of the as-synthesized MXenes

The quality of the synthesized MXenes was studied by high-resolution transmission electron microscopy (HR-TEM, *Tecnai F20, FEI*) using an acceleration voltage of 200 kV. The surface chemistry and surface terminations of the nano-sheets were investigated by Raman spectroscopy and X-ray diffraction (XRD). Concerning Raman spectroscopy (*Alpha 300 RA, Witec*), an excitation wavelength of 633 nm, a grating of 300 g mm⁻¹ and 10% of the maximum laser intensity were used. The spectra were collected using an integration time of 4 seconds and 256 accumulations. The phase analysis was done in a powder diffractometer using a Bragg-Brentano configuration (*PANalytical Empyrean*) operating at 40 kV and 40 mA with CuK_α irradiation ($\lambda = 0.15406$ nm). The diffraction angle (2 Theta) was swept from 5 to 65°. The step size was 0.026° and the dwelling time at each measuring point was 1396.89 seconds.

2.3. Preparation of MXenes-SnO₂ precursor solution

MXenes-SnO₂/Ti electrodes were fabricated by spin coating of Ti substrates using a precursor solution prepared by the method proposed by Pechini [15]. The precursor solution was prepared by dissolving 1.89 g of citric acid (C₆H₈O₇, Sigma-Aldrich, 99.5% purity) in 3.4 mL of ethylene glycol (C₂H₆O₂, Merck, 99.5% purity) at 60 °C. Afterwards, the citric acid solution was heated to 90 °C and 529 mg of tin chloride (II) (SnCl₂·2H₂O, Merck, 98.0% purity) were added to the aforementioned solution. The solution was stirred until reaching the complete dissolution of the precursors. After having cooled down to room temperature, 6 mg of MXenes were added to the mixture to obtain the MXenes-SnO₂ precursor solution.

2.4. Fabrication of MXenes-SnO₂ electrodes

For the fabrication of MXenes-SnO₂/Ti electrodes, Ti plates (99.8% purity) with dimensions of 1 cm x 1.5 cm x 0.5 mm were pre-treated by polishing their surface with emery paper in successive grits of 600, 1500 and 2000. The polished substrates were consecutively cleaned in acetone, ultra-pure water and absolute ethanol. Afterwards, the precursor solution was ultrasonically stirred for 20 minutes and the Ti plates were modified by adding 40 μL of the precursor solution onto their surfaces and spin coating the samples at 3000 rpm for 1 minute. Each electrode was dried at 70 °C for 10 minutes before applying the next layer. Every 5 layers, the electrodes were thermally treated in a Nabertherm LHTCT 01/16 box furnace at 400 °C for 10 minutes, following the subsequent procedure: using a heating rate of 5 °C min⁻¹ the temperature was increased to 130 °C and samples were kept at this temperature for 30 minutes to remove water; afterwards, the temperature was increased to 250 °C and maintained for 10 minutes to eliminate organic materials leading to the formation of the metal oxide films; finally, the temperature

was increased to 400 °C and maintained for 10 minutes. At the end of this process, the furnace was switched off and left to cool down naturally with the electrode samples inside. The coating cycle was repeated 8 times to achieve a total number of 40 layers. During the final cycle, electrodes were maintained at 400 °C for 2 hours to ensure the formation of metal oxides.

2.5. Characterization of the MXenes-SnO₂ electrodes

The surface morphology of the electrodes was characterized by scanning electron microscopy (SEM), which was performed using a FEI microscope (Quanta 250 FEG). The chemical composition was analysed by energy-dispersive X-ray spectroscopy (EDX) using an acceleration voltage of 20 kV. The crystallinity of the electrodes was characterized by grazing angle XRD analysis (Bruker D8 Advance diffractometer) with CuK α radiation ($\lambda=0.15406$ nm) and working at 30 kV / 40 mA in a scanning angle (2 Theta) range from 20 to 80° with a step size of 0.02°. Raman spectra were collected at room temperature (LabRAM HR Evolution) using an excitation wavelength of 633 nm within a Raman shift between 200 and 900 cm⁻¹.

2.6. Electrochemical performance of the MXenes-SnO₂ electrodes

The electrocatalytic behaviour of the MXenes-SnO₂ electrodes was studied by cyclic voltammetry, methyl red (MR) electro-oxidation and electrochemical impedance spectroscopy (EIS) experiments using a Gamry Reference 3000 potentiostat/galvanostat/ZRA. To this end, it was used a three electrodes system consisting of a 100 mL jacketed glass cell, the fabricated MXenes-SnO₂ anodes as working electrodes (with a geometric area of 1 cm²), a platinum wire as counter electrode and an Ag/AgCl (3 M KCl) reference electrode¹. Cyclic voltammetry experiments were performed using 50 mL of a 0.1 M sodium sulfate (Na₂SO₄, Merck, 99.0% purity) solution as electrolyte at constant 25 °C, along with 10 mg L⁻¹ of methyl red as required. For each electrode, it was used a potential range between its open circuit potential and 1.7 V at a scan rate of 25 mV s⁻¹ with a step size of 10 mV. All measurements were repeated at least three times to confirm the reproducibility of the results.

For the electrocatalytic degradation experiments, 50 mL of a 10 mg L⁻¹ methyl red (C₁₅H₁₅N₃O₂, Merck), 1 M sulfuric acid (H₂SO₄, Merck) and 20 mM sodium sulfate (Na₂SO₄, Merck) aqueous solution were used as electrolyte. The degradation of methyl red was performed for 5 hours under potentiostatic conditions, applying a constant potential of 2.5 V to the working electrode while keeping the temperature constant at 25 °C. Samples were taken every 60 minutes to measure the concentration of methyl red in the electrolyte using an UV-visible spectrophotometer (Agilent 8553 UV-visible spectrometer) at $\lambda_{\max}=517$ nm. The fraction of dye degradation (C_t/C_0) was calculated using equation (1):

$$C_t/C_0 = \frac{Abs_t}{Abs_0} \quad (1)$$

where Abs_0 and Abs_t are the electrolyte absorbances at t_0 (initial absorbance) and t , respectively.

¹ All the potentials presented in this work are referred to this electrode, unless noted otherwise.

For EIS measurements, a potential of 2.5 V was applied to the working electrode with a perturbation signal with 10 mV AC amplitude. Frequencies analysed were between 100 kHz and 0.1 Hz in 50 mL of a 10 mg L⁻¹ methyl red (C₁₅H₁₅N₃O₂, Merck), 1 M sulfuric acid (H₂SO₄, Merck) and 20 mM sodium sulfate (Na₂SO₄, Merck) electrolyte.

3. RESULTS AND DISCUSSION

3.1. Characterization of the as-synthesized MXenes

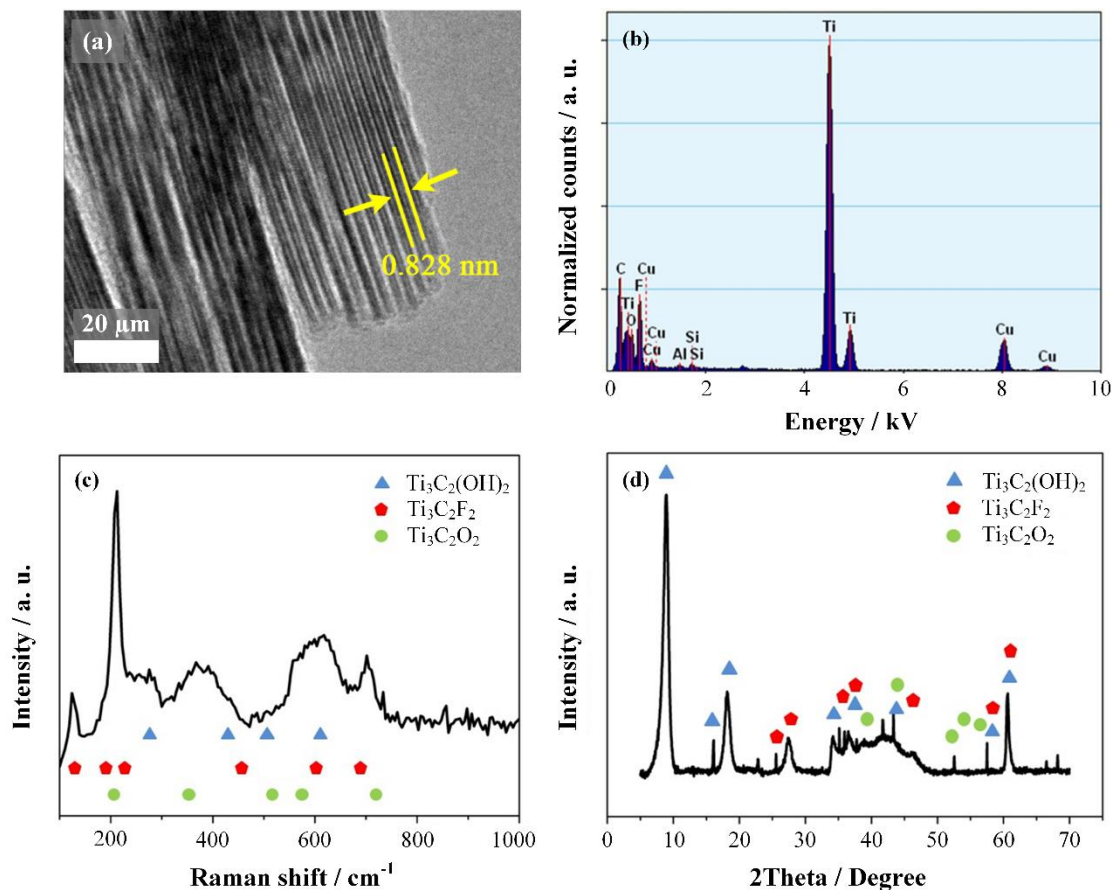


Figure 1. (a) HR-TEM micrograph, (b) TEM-EDX spectrum, (c) Raman spectrum and (d) XRD pattern of the as-synthesized MXenes

Error! Reference source not found.a shows an HR-TEM micrograph of the as-synthesized MXenes, which reveals their regular multi-layered structure having a layer distance of about 0.828 nm. The TEM-EDX analysis presented in **Error! Reference source not found.**b confirms that titanium, carbon, oxygen and fluorine are the main chemical elements present in Ti₃C₂T_x nano-sheets. The multi-layered MXene nano-sheets contain about 80-100 layers with x-y-dimensions in the order of a few microns (between 1.5-2 microns). Negligible traces of aluminum (0.3 wt.%) were found, which stem from the original MAX-phase. The Raman spectrum depicted in **Error! Reference source not found.**c shows pronounced peaks at 125, 212 and 701 cm⁻¹, as well as broad peaks around 285, 376 and 600 cm⁻¹. These vibrations can be directly associated to Ti₃C₂O₂, Ti₃C₂F₂ and Ti₃C₂(OH)₂ [16–19]. This is

confirmed by the peaks observed in the XRD pattern shown in **Error! Reference source not found.d**, which can be also associated with the same surface terminations, namely -O, -F and -OH groups [18]. The most dominant peaks – located at fairly low diffraction angles – can be assigned to hydroxyl (-OH) terminations, followed by less pronounced -F and -O contributions. The occurrence of these terminations verified by Raman spectroscopy and XRD can be traced back to the aluminum etching process using concentrated HF. A complete characterization of the as-synthesized MXenes can be found in previous work [20].

3.2. Characterization of the MXenes-SnO₂ electrodes

3.2.1. SEM and EDX analysis

Error! Reference source not found. shows SEM micrographs of the surfaces of the MXenes-SnO₂ electrodes. As can be seen in **Error! Reference source not found.a**, (pure) MXenes/Ti electrodes present a rather rough surface with no clear sign of MXenes on it. In contrast, **Error! Reference source not found.b** shows that (pure) SnO₂/Ti electrodes exhibit delamination of the SnO₂ layers, which may be connected to the high number of coated layers on the Ti plate (40 layers). As can be seen in **Error! Reference source not found.c**, the addition of MXenes to the SnO₂ coating (MXenes-SnO₂/Ti electrodes) has a significant impact on the electrodes surface topography, since an irregular and fine “mud-cracks” morphology can be observed. This “mud-cracks” morphology is characteristic of thermally prepared coatings on titanium substrates – due to different thermal expansion coefficients of the film and titanium [21] – and favours the electrodes catalytic activity, increases their electroactive area and enhances their corrosion resistance [21,22]. The elemental mapping obtained showed a uniform distribution of all the elements on the substrate surfaces (**Error! Reference source not found.d**).

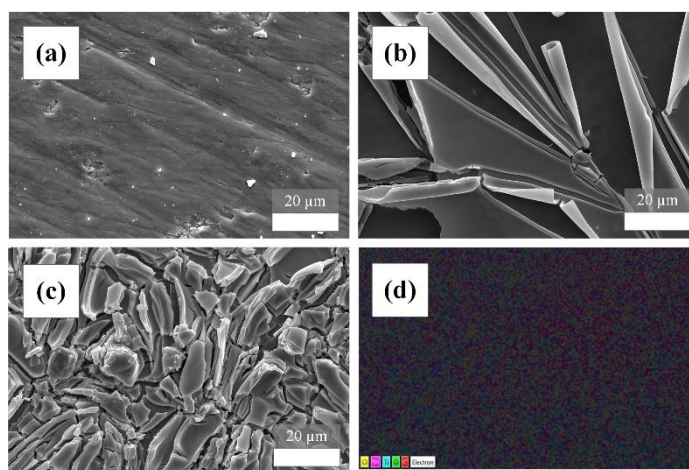


Figure 2 SEM micrographs of (a) MXenes/Ti, (b) SnO₂/Ti, (c) MXenes-SnO₂/Ti and (d) EDX elemental mapping of MXenes-SnO₂/Ti electrodes

The chemical composition of each electrode surface, determined by EDX, is summarized in **Error! Reference source not found.**. Regarding the Ti content, it decreases consistently for SnO₂/Ti

and MXenes-SnO₂/Ti, which can be associated with the more regular surface morphology observed in the SEM micrographs for MXenes-SnO₂/Ti electrodes. This also could explain the slight differences in the contents of carbon and tin in the samples.

Table 1. Chemical composition of MXenes/Ti, SnO₂/Ti and MXenes-SnO₂/Ti electrodes determined by EDX analysis.

Electrode	EDX value / wt. %			
	Ti	O	C	Sn
MXenes/Ti	68.60	29.12	2.28	–
SnO ₂ /Ti	15.15	13.18	2.04	63.63
MXenes-SnO ₂ /Ti	2.19	11.06	2.30	84.45

* the elemental mapping of the electrodes surface showed a uniform elemental distribution on it

3.2.2. Raman spectroscopy

Since MXenes-SnO₂ electrodes are thermally treated at 400 °C at the final fabrication stage under ambient atmospheric conditions, it can be expected that MXenes are partially or completely oxidised to TiO₂ rutile nano-crystals [8,9]. This decomposition was confirmed by thermogravimetric analysis of the synthesized MXenes in air (between 25 and 500°C using a NETZSCH TG 209 F1 Libra apparatus) and Raman spectroscopy analysis of the MXenes-SnO₂ electrodes. **Error! Reference source not found.** summarizes the Raman spectra obtained for MXenes/Ti, SnO₂/Ti and MXenes-SnO₂/Ti electrodes. For the MXenes/Ti electrodes, the assignment of the Raman bands can be ascribed to a TiO₂ rutile phase, formed on the surface of the Ti substrate during the thermal treatment, with peaks at 447 and 612 cm⁻¹, which correspond to the E_g and A_{1g} vibration modes of TiO₂, respectively [23].

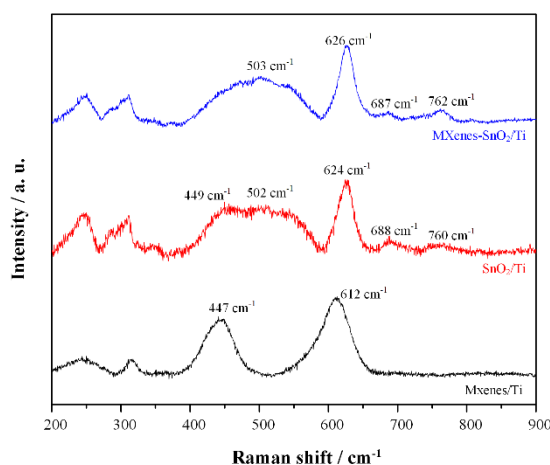


Figure 3. Summary of the measured Raman spectra of MXenes/Ti, SnO₂/Ti and MXenes-SnO₂/Ti electrodes

Regarding the SnO₂/Ti electrodes, it is important to point out that SnO₂ crystallizes with a rutile structure, which belongs to the centrosymmetric group D_{4h}¹⁴. Therefore, this solid is expected to present

three main vibration modes (A_{1g} , B_{2g} and E_g) in the Raman spectra with frequencies for solid single crystals located at 634, 776 and 475 cm^{-1} , respectively [24,25]. As mentioned before, the main bands of TiO_2 are located at 447 and 612 cm^{-1} , which implies that the SnO_2 rutile peaks are positioned at similar frequencies. The presence of SnO_2 on the surface of SnO_2/Ti electrodes as a separated phase could be perceived as a shift in frequency of the peaks associated with A_{1g} and E_g modes of TiO_2 rutile. Moreover, it is worth to mention that this frequency shift can also result from suboxidic mixtures or an increase of disorder due to Sn ions doping the TiO_2 structure [26,27]. A detailed inspection of the spectrum obtained for the SnO_2/Ti electrodes reveals the appearance of a considerably broad peak centred at 502 cm^{-1} , which can be ascribed to the A_{2u} mode of SnO_2 [25]. Together with the presence of bands corresponding to the B_{2g} and E_{g2} modes of SnO_2 present at 760 and 688 cm^{-1} , respectively, this result suggests that SnO_2 appears as a separate crystalline phase instead of metal ions doped into the TiO_2 lattice. This supports the premise of the bands assigned to SnO_2 being overlapped with the crystalline plane of TiO_2 [28]. Additional peaks can be observed at low frequencies, which could be attributed to vibrational modes of oxygen vacancy-related defects [29].

Concerning the effect of the incorporation of MXenes into the structure of SnO_2/Ti electrodes, it can be seen that $\text{Ti}_3\text{C}_2\text{T}_x$ nano-sheets exert an effect on the frequencies of the fundamental vibrations in the MXenes- SnO_2/Ti electrode (**Error! Reference source not found.**). A general shift of the vibrational modes to higher frequencies and a decrease of the intensity of the E_g mode of SnO_2 (translational) peak can be observed. The frequencies shift associated with the vibration modes can be related to the formation of TiO_2 rutile nano-crystals [8,9], thus generating an increase of the disordered structures and boundaries in the film. Additionally, the decrease in the intensity of E_g mode of SnO_2 may be associated with the incorporation of Ti cations into the lattice of SnO_2 . Since Ti^{4+} ions (with a radius of 0.68 Å) are slightly smaller than Sn^{4+} ions (0.71 Å), the bonds of the Ti^{4+} ion that replaces Sn^{4+} in the lattice of SnO_2 are slightly longer than the original bonds thus generating a change in the vibrational mode.

3.2.3. XRD analysis

The XRD analysis of the MXenes- SnO_2/Ti electrodes is presented in **Error! Reference source not found.** The diffractogram of MXenes- SnO_2/Ti electrodes confirms the presence of the tetragonal rutile structure of SnO_2 as a separated phase from TiO_2 (PDF# 01-072-1147), which presents peaks at 26.75, 33.89, 38.40, 52.04, 54.63, 58.14, 62.08 and 62.96°, corresponding to the (110), (101), (200), (211), (220), (002), (310) and (221) reflection planes, respectively. Particularly, the peak located at 26.75° associated with the (110) plane is the most intense peak, which suggests the preferred crystallographic orientation. Additionally, the peaks associated with the rutile TiO_2 phase (PDF# 01-087-0710) with strong interference of the Ti metallic substrate can be seen in **Error! Reference source not found.** (PDF# 01-089-3725).

In summary, the results of surface characterization of the fabricated electrodes indicate the formation of a $\text{SnO}_2\text{-TiO}_2$ film on the surface of the Ti plates with a rough morphology. Furthermore, the addition of MXenes leads to the formation of TiO_2 rutile nano-crystals in the films structure and the incorporation of Ti^{4+} ions into the lattice of SnO_2 crystals.

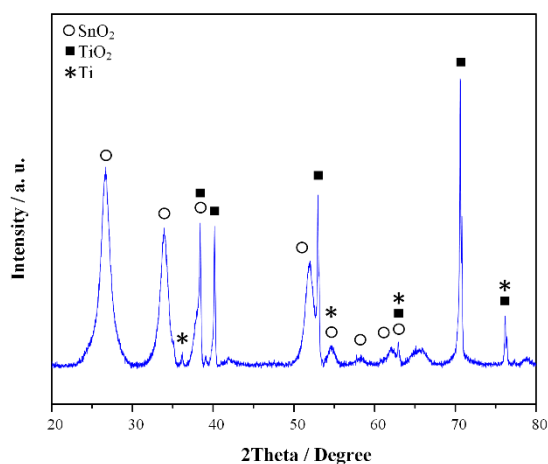


Figure 4 XRD patterns of the MXenes-SnO₂/Ti electrodes

3.3. Electrochemical performance of the MXenes-SnO₂ electrodes

3.3.1. Electrocatalytic activity for the oxygen evolution reaction

Electrode materials with a low activity for the oxygen evolution reaction (OER) are greatly desirable for electrochemical advanced oxidation applications, since the current density efficiency for water pollutant oxidation processes on the anode surface is reduced by its simultaneous occurrence on it [30].

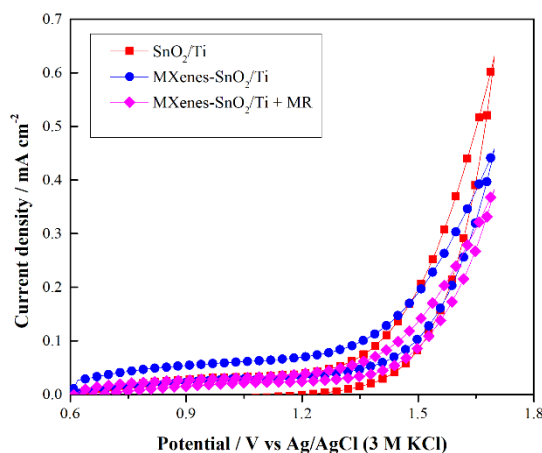


Figure 5 Voltammograms obtained for SnO₂/Ti and MXenes-SnO₂/Ti anodes immersed in 0.1 M sodium sulfate and MXenes-SnO₂/Ti anodes immersed in 0.1 M sodium sulfate along with 10 mg L⁻¹ of methyl red.

Error! Reference source not found. shows the voltammograms obtained for SnO₂/Ti and MXenes-SnO₂/Ti anodes immersed in 0.1 M sodium sulfate, which characterize the OER kinetics on these electrodes. As can be seen, noticeable differences occur between the current densities associated

with each electrode and a higher current density is observed for the SnO₂/Ti electrodes. This result suggests a lower activity for the OER on the MXenes-SnO₂/Ti electrodes compared to that on SnO₂/Ti electrodes, which would positively affect the current density efficiency of water pollutant oxidation processes (see section 3.3.2 for further discussion). Additionally, the voltammogram obtained for MXenes-SnO₂/Ti anodes immersed in 0.1 M sodium sulfate along with 10 mg L⁻¹ of methyl red shows no additional peaks compared to the behaviour of the electrodes in the absence of the organic compound. This indicates that direct electron transfer does not occur at the anode surface, as expected for non-active electrodes (electrochemical oxidation mediated by hydroxyl radicals) such as SnO₂/Ti and MXenes-SnO₂/Ti anodes [31].

3.3.2. Electrocatalytic activity for the oxidation of methyl red

EAOPs are based upon the generation of highly reactive oxidants, mostly hydroxyl radicals (•OH) [32]. It is known that the redox reaction for the •OH formation has one of the highest standard potentials among oxidants: to promote the generation of •OH from the oxidation of water molecules (reaction (2)) at pH = 0, a potential above $E_{OH_{aq}/H_2O}^0 = 2.59$ V vs SHE must be applied [4]. Consequently, the application of a constant potential of 2.5 V vs Ag/AgCl (3 M KCl) – equivalent to 2.71 V vs SHE – ensures the formation of free •OH radicals in the electrochemical cell.



Considering that free •OH radicals are the main responsible for organic degradation at the surface of non-active electrodes, as it is the case for SnO₂-based electrodes, this anodic potential value was adequate for the purposes of this research work and in addition it is associated to a minimal energy consumption due to its proximity to the standard potential for water oxidation [31].

The methyl red (MR) degradation curves obtained using the SnO₂/Ti and MXenes-SnO₂/Ti anodes are shown in **Error! Reference source not found.**. The fractions of dye degradation (C_t/C_0) measured after 5 hours of treatment (under potentiostatic conditions) are approximately 0.65 and 0.60 for the SnO₂/Ti and MXenes-SnO₂/Ti anodes, respectively. The average current densities measured during these processes were ca. 6.57 mA cm⁻² and 10.26 mA cm⁻² for the SnO₂/Ti and MXenes-SnO₂/Ti anodes, respectively. Additionally, the MR degradation kinetics at a constant potential were fitted using the following pseudo-first-order model:

$$-\ln\left(\frac{Abs_t}{Abs_0}\right) = Kt \quad (3)$$

where Abs_0 is the initial electrolyte absorbance (measured in a 10 mg L⁻¹ MR aqueous solution containing 1 M H₂SO₄ and 20 mM Na₂SO₄), Abs_t is the electrolyte absorbance at time t , and K is the rate constant for the degradation reaction.

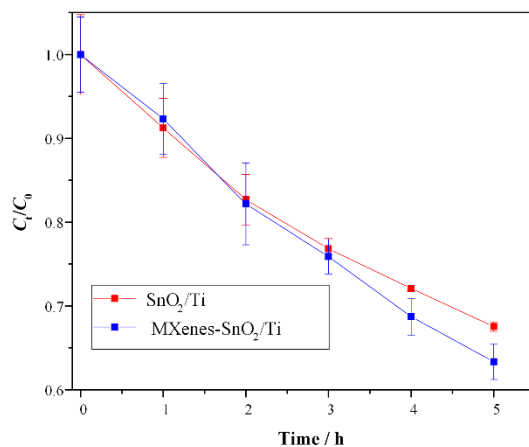


Figure 6. Methyl red degradation transients obtained using SnO₂/Ti and MXenes-SnO₂/Ti anodes (applied potential: 2.5 V vs Ag/AgCl (3 M KCl), counter electrode: platinum wire, electrolyte: C₀=10 mg L⁻¹ of MR in an aqueous solution containing 1 M H₂SO₄ and 20 mM Na₂SO₄)

The calculated first-order constants for the MR degradation reaction are 0.085 h⁻¹ and 0.101 h⁻¹ (both with a determination coefficient R² = 0.99) for the SnO₂/Ti and MXenes-SnO₂/Ti anodes, respectively. The maximum rate constant for MR degradation corresponds to the system with the MXenes-SnO₂/Ti anode, which is 19% higher than the value obtained for the system with the SnO₂/Ti anode. As discussed previously, the incorporation of Ti₃C₂T_x nano-sheets to the SnO₂/Ti electrode led to the formation of a Ti-doped SnO₂ structure, with Ti cations occupying substitutional positions. This doped structure allows for the generation of oxygen vacancies in the crystal lattice, which act as charge carriers and increase the electrical conductivity of SnO₂ [33]. Therefore, it can be inferred that the enhanced activity of the MXenes-SnO₂/Ti electrode for the degradation of MR is related to the increase in the concentration of charge carriers on the SnO₂ structure.

3.3.3. Electrochemical charge transfer resistance

The effect of MXenes on the electrochemical behaviour of SnO₂/Ti anodes during the electro-oxidation of MR was further studied by electrochemical impedance spectroscopy (EIS) analysis. Fig. 7a shows the EIS Nyquist plots obtained for SnO₂/Ti and MXenes-SnO₂/Ti anodes. The spectra were fitted to the equivalent circuit model in Fig. 7b using the Gamry Echem Analyst software v6.23, applying the Simplex method in the curve fitting toolbox. This equivalent circuit model has been reported elsewhere for the electro-oxidation of organic compounds using SnO₂-based anodes [34,35], where R_s represents the solution resistance, R_{ct} is the charge transfer resistance, and CPE is a constant phase element which describes the double-layer capacitance of the solution-electrode interface (with parameters Y⁰ and α). The values of the fitted parameters associated with each circuit element are listed in Table 2. The Good of Fit (GoF) of experimental and simulated data display a value of 7.75·10⁻³ and 4.63·10⁻³ for SnO₂/Ti and MXenes-SnO₂/Ti anodes, respectively. These values suggest that the proposed circuit is suitable for effective fitting of the experimental data.

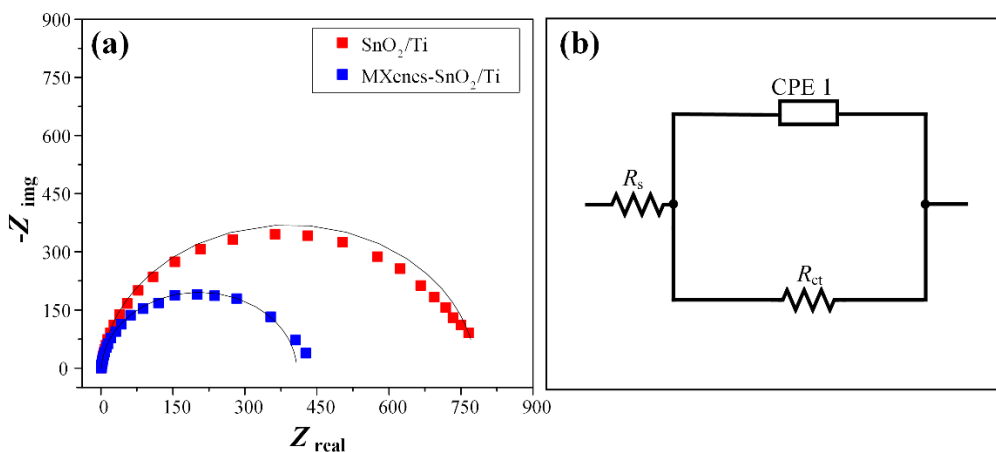


Figure 7. (a) EIS Nyquist plots obtained during the electrochemical degradation of methyl red using SnO₂/Ti and MXenes-SnO₂/Ti anodes ($C_0=10 \text{ mg L}^{-1}$ of MR in an aqueous solution containing 1 M H₂SO₄ and 20 mM Na₂SO₄) and (b) electrochemical equivalent circuit model proposed

Table 2. Fitted parameters for each equivalent circuit element associated with the electrochemical performance of SnO₂/Ti and MXenes-SnO₂/Ti anodes.

Electrode	R_s / Ω	R_{ct} / Ω	$Y^0 / \text{S}\cdot\text{s}^a$	a	GoF
SnO ₂ /Ti	1.07	780.7	$6.98 \cdot 10^{-6}$	0.96	$7.75 \cdot 10^{-3}$
Mxenes-SnO ₂ /Ti	1.25	406.8	$8.83 \cdot 10^{-6}$	0.98	$4.63 \cdot 10^{-3}$

It is worth to note that EIS data were tested and validated using Kramers-Kronig transforms (KKTs), obtaining a maximum residual error lower than 0.06% for all experiments. Detailed information on the formulation of KKTs can be found elsewhere [36,37].

As can be seen in Table 2, the MXenes-SnO₂/Ti electrodes display a considerably lower (ca. -50%) charge transfer resistance compared with SnO₂/Ti electrodes. In addition, the a -values obtained for the CPE elements suggest an almost pure capacitive behaviour for both SnO₂/Ti and MXenes-SnO₂/Ti electrodes, with calculated CPEs of 5.62 μF and 5.15 μF for the MXenes-SnO₂/Ti and SnO₂/Ti anodes, respectively. This similarity between the CPE values of both electrodes suggests that they present comparable specific reaction areas [35,38], which confirms that the incorporation of Ti into the crystal lattice of SnO₂ affects primarily the charge transfer resistance (electrical conductivity) of the SnO₂-based anodes as discussed in Sections 3.3.1 and 3.3.2.

4. CONCLUSIONS

MXenes-SnO₂ electrodes were fabricated by spin-coating of a precursor solution on Ti substrates and their surface composition and electrochemical behaviour were studied. The surface characterization of these electrodes suggests the formation of SnO₂-TiO₂ films with presence of TiO₂ rutile nano-crystals and Ti⁴⁺ ions incorporated into the lattice of SnO₂ crystals due to the thermal treatment of the electrodes

at 400 °C under ambient atmospheric conditions in the final stages of their fabrication. MXenes-SnO₂/Ti electrodes restrained the oxygen evolution reaction and showed enhanced kinetics for the electro-oxidation of methyl red compared to the performance of (pure) SnO₂/Ti electrodes, probably due to the presence of oxygen vacancies in the Ti-doped SnO₂ structure which decrease by nearly a 50% the electrodes charge transfer resistance (determined by electrochemical impedance spectroscopy analysis).

ACKNOWLEDGMENTS

The authors thank ANID for a Beca Doctorado Nacional, Ph.D. Scholarship N° 21180182, for Sergio González-Poggini, and to Claudia Cannatelli from the Raman Laboratory (Lab-RAM) of the Department of Geology, Universidad de Chile, for her collaboration in the Raman analyses (ANID Fondecip Program EQM170103). Andreas Rosenkranz greatly acknowledges the financial support given by ANID within the project Fondecyt 11180121 as well as the VID of the Universidad de Chile in the framework of “U-Inicia UI013/2018”. Finally, Samuel Hevia acknowledges the FONDEQUIP EQM 150101.

References

1. F.C. Moreira, R.A.R. Boaventura, E. Brillas, V.J.P. Vilar, *Appl. Catal. B Environ.*, 202 (2017) 217–261.
2. S. Garcia-Segura, J.D. Ocon, M.N. Chong, *Process Saf. Environ. Prot.*, 113 (2018) 48–67.
3. A.N. Subba Rao, V.T. Venkatarangaiah, G.B. Nagarajappa, S.H. Nataraj, P.M. Krishnegowda, *J. Environ. Chem. Eng.*, 5 (2017) 4969–4979.
4. W. Wu, Z.H. Huang, T.T. Lim, *Appl. Catal. A Gen.*, 480 (2014) 58–78.
5. A. Chen, S. Xia, H. Pan, J. Xi, H. Qin, H. Lu, Z. Ji, *J. Electroanal. Chem.*, 824 (2018) 169–174.
6. S. Venkateshalu, A.N. Grace, *Appl. Mater. Today*, 18 (2020) 100509.
7. R. Li, L. Zhang, L. Shi, P. Wang, *ACS Nano*, 11 (2017) 3752–3759.
8. Z. Li, L. Wang, D. Sun, Y. Zhang, B. Liu, Q. Hu, A. Zhou, *Mater. Sci. Eng. B Solid-State Mater. Adv. Technol.*, 191 (2015) 33–40.
9. M. Naguib, O. Mashtalir, M.R. Lukatskaya, B. Dyatkin, C. Zhang, V. Presser, Y. Gogotsi, M.W. Barsoum, *Chem. Commun.*, 50 (2014) 7420–7423.
10. Y. Gao, L. Wang, A. Zhou, Z. Li, J. Chen, H. Bala, Q. Hu, X. Cao, *Mater. Lett.*, 150 (2015) 62–64.
11. Y. Gao, H. Chen, A. Zhou, Z. Li, F. Liu, Q. Hu, L. Wang, *Nano*, 10 (2015) 1550064.
12. N. Li, Y. Zhang, M. Jia, X. Lv, X. Li, R. Li, X. Ding, Y.Z. Zheng, X. Tao, *Electrochim. Acta*, 326 (2019) 1–9.
13. M. Yu, Z. Wang, J. Liu, F. Sun, P. Yang, J. Qiu, *Nano Energy*, 63 (2019) 103880.
14. J.J. Huang, X.Q. Liu, F.F. Meng, L.Q. He, J.X. Wang, J.C. Wu, X.H. Lu, Y.X. Tong, P.P. Fang, *J. Electroanal. Chem.*, 856 (2020) 113727.
15. M.P. Pechini, US Patent# 3.330. 697, 1967.
16. X. Zhang, Y. Liu, S. Dong, Z. Ye, Y. Guo, *Ceram. Int.*, 43 (2017) 11065–11070.
17. T. Hu, J. Wang, H. Zhang, Z. Li, M. Hu, X. Wang, *Phys. Chem. Chem. Phys.*, 17 (2015) 9997–10003.
18. M. Hu, T. Hu, Z. Li, Y. Yang, R. Cheng, J. Yang, C. Cui, X. Wang, *ACS Nano*, 12 (2018) 3578–3586.
19. A. Sarycheva, Y. Gogotsi, *Chem. Mater.* 32 (2020) 3480–3488.
20. A. Rosenkranz, P.G. Grützmaier, R. Espinoza, V.M. Fuenzalida, E. Blanco, N. Escalona, F.J. Gracia, R. Villarroel, L. Guo, R. Kang, F. Mücklich, S. Suarez, Z. Zhang, *Appl. Surf. Sci.*, 494

- (2019) 13–21.
21. J. tao Kong, S. yuan Shi, X. ping Zhu, J. ren Ni, *J. Environ. Sci.*, 19 (2007) 1380–1386.
 22. C.F.C. Machado, M.A. Gomes, R.S. Silva, G.R. Salazar-Banda, K.I.B. Eguiluz, *J. Electroanal. Chem.*, 816 (2018) 232–241.
 23. U. Balachandran, N.G. Eror, *J. Solid State Chem.*, 42 (1982) 276–282.
 24. M. Ocaña, C.J. Serna, J. V. García-Ramos, E. Matijević, *Solid State Ionics*, 63–65 (1993) 170–177.
 25. S.S. Chang, M.S. Jo, *Ceram. Int.*, 33 (2007) 511–514.
 26. Z. Jiang, Z. Guo, B. Sun, Y. Jia, M. Li, J. Liu, *Sensors Actuators, B Chem.*, 145 (2010) 667–673.
 27. F. Edelman, H. Hahn, S. Seifried, C. Aloff, H. Hoche, A. Balogh, P. Werner, K. Zakrzewska, M. Radecka, P. Pasierb, A. Chack, V. Mikhelashvili, G. Eisenstein, *Mater. Sci. Eng. B Solid-State Mater. Adv. Technol.*, 69 (2000) 386–391.
 28. G. Yang, Z. Yan, T. Xiao, *Appl. Surf. Sci.*, 258 (2012) 8704–8712.
 29. V.G. Kravets, L. V. Poperenko, *J. Appl. Phys.*, 103 (2008) 1–7.
 30. C. Comninellis, G. Chen, *Electrochemistry for the Environment*, first ed., Springer, (2010) New York.
 31. G. Kreysa *et al.*, *Encyclopedia of Applied Electrochemistry*, Springer, (2014) New York.
 32. P. V. Nidheesh, M. Zhou, M.A. Oturan, *Chemosphere*, 197 (2018) 210–227.
 33. X.M. Liu, S.L. Wu, P.K. Chu, J. Zheng, S.L. Li, *Mater. Sci. Eng. A*, 426 (2006) 274–277.
 34. C. Shao, F. Zhang, X. Li, J. Zhang, Y. Jiang, H. Cheng, K. Zhu, *J. Electroanal. Chem.*, 832 (2019) 436–443.
 35. L. Pahlevani, M.R. Mozdianfard, N. Fallah, *J. Water Process Eng.*, 35 (2020) 101204.
 36. B. Boukamp, *Solid State Ionics*, 62 (1993) 131–141.
 37. M. Schönleber, D. Klotz, *Electrochim. Acta*, 131 (2014) 20–27.
 38. A. Nanjanagudu Subba Rao, V. Thimmappa Venkatarangiah, *Mater. Today Proc.*, 5 (2018) 25006–25015.